JACS
JOURNAL OF THE AMERICAN CHEMICAL SOCIETY
Article
pubs.acs.org/JACS

Synthesis, Characterization, and Transistor and Solar Cell Applications of a Naphthobisthiadiazole-Based Semiconducting Polymer

Itaru Osaka,*[,†,‡] Masafumi Shimawaki,[†] Hiroki Mori,[†] Iori Doi,[†] Eigo Miyazaki,[†] Tomoyuki Koganezawa,[§] and Kazuo Takimiya*[,†,¶]

[†]Department of Applied Chemistry, Graduate School of Engineering, Hiroshima University, 1-4-1 Kagamiyama, Higashi-Hiroshima, Hiroshima 739-8527, Japan

[‡]Precursory Research for Embryonic Science and Technology (PRESTO), Japan Science and Technology Agency, Chiyoda-ku 102-0075, Japan

[§]Japan Synchrotron Radiation Research Institute, 1-1-1, Kouto, Sayo-cho, Sayo-gun, Hyogo 679-5198, Japan

[¶]Institute for Advanced Materials Research, Hiroshima University, Higashi-Hiroshima 739-8530, Japan

Supporting Information

ABSTRACT: We report the synthesis and characterization of a novel donor−acceptor semiconducting polymer bearing naphthobisthiadiazole (NTz), a doubly benzothiadiazole (BTz)-fused ring, and its applications to organic field-effect transistors and bulk heterojunction solar cells. With NTz's highly π-extended structure and strong electron affinity, the NTz-based polymer (PNTz4T) affords a smaller bandgap and a deeper HOMO level than the BTz-based polymer (PBTz4T). PNTz4T exhibits not only high field-effect mobilities of ~0.56 $cm^2/(V\,s)$ but also high photovoltaic properties with power conversion efficiencies of ~6.3%, both of which are significantly high compared to those for PBTz4T. This is most likely due to the more suitable electronic properties and, importantly, the more highly ordered structure of PNTz4T in the thin film than that of PBTz4T, which might originate in the different symmetry between the cores. NTz, with centrosymmetry, can lead to a more linear backbone in the present polymer system than BTz with axisymmetry, which might be favorable for better molecular ordering. These results demonstrate great promise for using NTz as a bulding unit for high-performance semiconducting polymers for both transistors and solar cells.

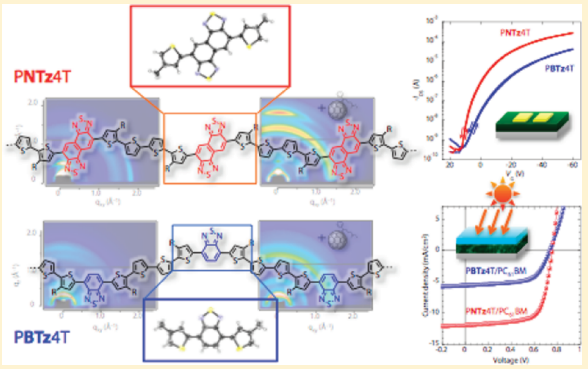

INTRODUCTION

Considerable attention has been given to semiconducting polymers in the field of organic electronics, because their solution processability, thermal stability, and mechanical properties allow access to large-area and flexible devices of next generations.[1] Organic field-effect transistors (OFETs) and solar cells are of particular interest today in the field. Recent advances in the development of new active materials, mostly small bandgap polymers with donor−acceptor (D−A) systems, have brought about great improvements in device performances, such as charge carrier mobilities of >1 $cm^2/(V\,s)$ in transistors[2] and power conversion efficiencies (PCEs) of >7% in solar cells.[3] A key issue for the development of high-performance materials is to build strong $\pi-\pi$ stacking structures, which facilitate charge carrier transport through π-orbital overlaps between cofacial polymer backbone.[1a,b,4] Thus, the choice of building units that ensure strong $\pi-\pi$ stacking is crucial for the design of high-performance polymers. Moreover, a versatile building unit that can be utilized for polymers with both high transistor and photovoltaic performances is highly desired for effective material development. However, among the number of building units studied for this class of polymers, such versatile units are not so many; cyclopentadithiophene (CDT),[5] benzodithiophene (BDT),[6] and indacenodithiophene (IDT)[2d,7] are examples of the donor unit, and benzothiadiazole (BTz, Figure 1),[5,8] thiazolothiazole (TzTz),[9] thienopyrrole-dione (TPD),[6c−e,10] diketopyrrolopyrrole (DPP),[11] and isoindigo (IID)[12] are examples of the acceptor unit. In particular, BTz is one of the first incorporated and most widely used acceptor units for high-performance D−A semiconducting polymers, owing to the strong electron affinity that offers deep HOMO energy levels and broad absorption ranges, which are important parameters for semiconducting polymers.[1h]

Naphtho[1,2-*c*:5,6-*c*′]bis[1,2,5]thiadiazole (NTz, Figure 1), a doubly BTz-fused heterocycle that was first synthesized by

Received: November 14, 2011
Published: January 17, 2012

   dx.doi.org/10.1021/ja210687r | *J. Am. Chem. Soc.* 2012, 134, 3498−3507

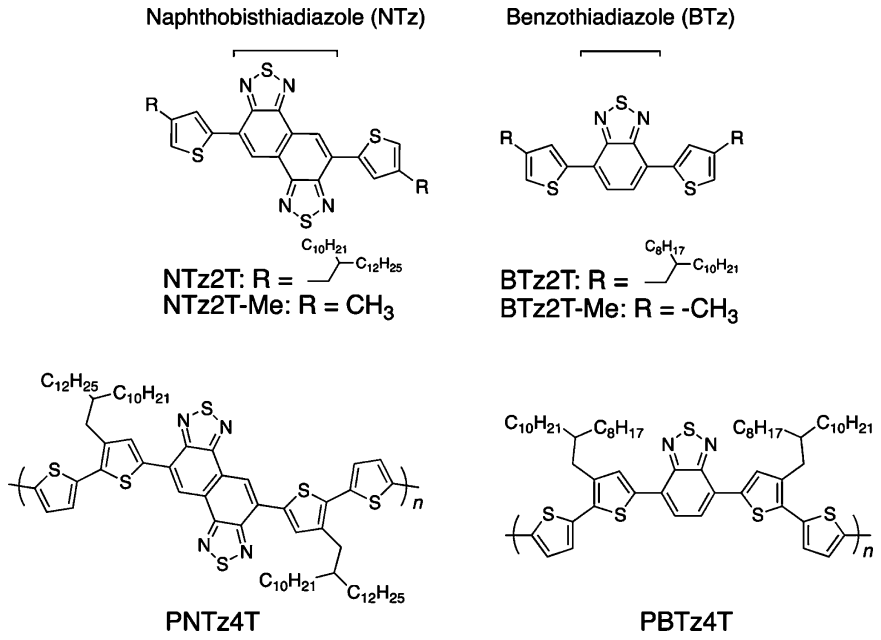

Figure 1. Chemical structures of naphtho[1,2-*c*:5,6-*c*′]bis[1,2,5]thiadiazole- and benzothiadiazole-based compounds (NTz2Ts and BTz2Ts) and semiconducting polymers (PNTz4T and PBTz4T) studied in this work.

Scheme 1. Synthetic Routes to the Polymers

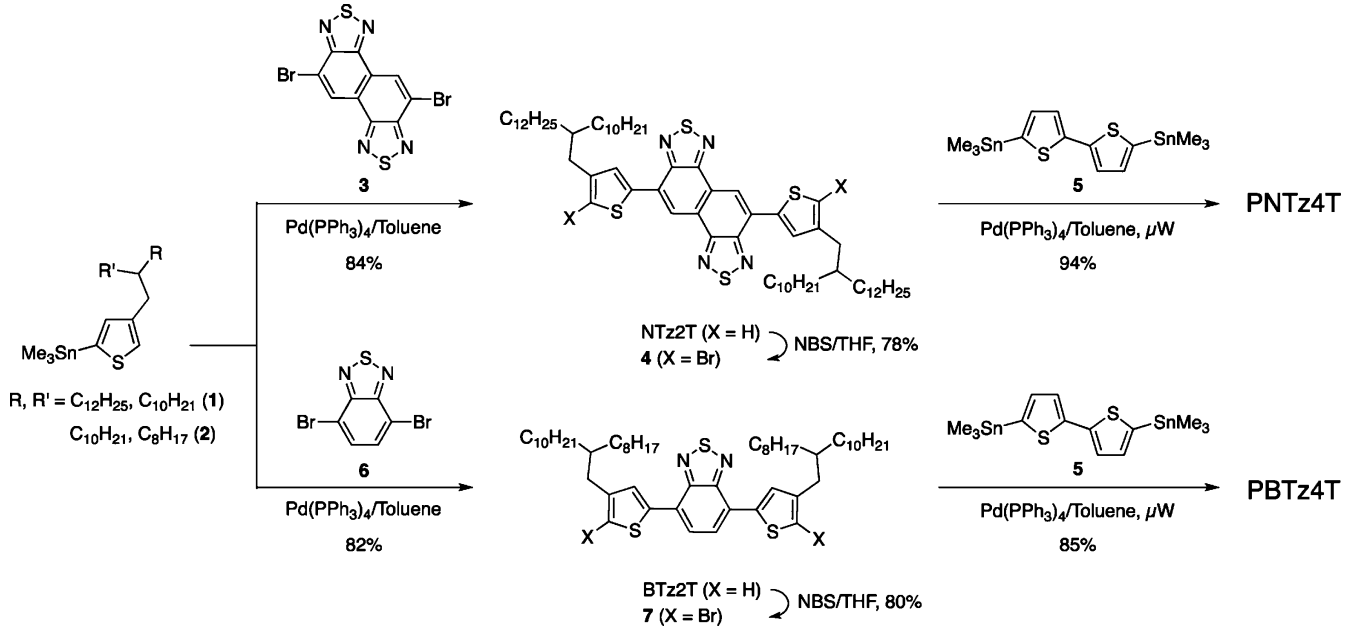

Mataka and co-workers in 1991,[13] could be a high-potential acceptor unit for semiconducting materials, because NTz is expected to be a stronger acceptor as well as a more π-extended ring as compared to BTz. Thus, the incorporation of NTz into the polymer main chain in combination with a donor unit could lead to deeper HOMO energy levels (E_{HOMO}) and smaller energy bandgaps (E_g). It can also enhance intermolecular interactions and thereby promote a strong $\pi-\pi$ stacking structure of polymer backbones due to the more rigid structure. In fact, during the course of this work, Huang, Cao, and co-workers reported on an NTz-based D−A semiconducting polymer incorporating a BDT moiety as the donor unit, which exhibits high PCEs of ~6.0% in solar cells.[14] Herein, we report the synthesis, characterization, and transistor and solar cell properties of a novel NTz-based semiconducting polymer, PNTz4T, in comparison with a BTz-based polymer, PBTz4T (Figure 1). A simple quaterthiophene moiety is chosen as the donor unit in the present case to clearly understand the nature of NTz in the semiconducting polymer. We first discuss the differences of the optical and electrochemical properties and the molecular structures between the monomer units of PNTz4T and PBTz4T (NTz2T and BTz2T), or between the corresponding model compounds (NTz2T-Me and BTz2T-Me), respectively (Figure 1). We then show the physicochemical properties, device characterizations, and ordering structures of the polymers (PNTz4T and PBTz4T) in the thin film and finally discuss the overall structure−property relationships.

dx.doi.org/10.1021/ja210687r | *J. Am. Chem. Soc.* 2012, 134, 3498−3507

RESULTS AND DISCUSSION

Synthesis and Thermal Property. Synthetic routes to the polymers are shown in Scheme 1. 3-(2-Decyltetradecyl)-5-trimethylstannylthiophene (**1**) and 4,9-dibromonaphtho[1,2-*c*:5,6-*c*′]bis[1,2,5]thiadiazole (**3**) were cross-coupled using the Migita−Kosugi−Stille reaction to afford NTz2T, which was then dibrominated with NBS to yield comonomer **4**. **4** and distannylated bithiophene (**5**) were copolymerized using a microwave-assisted reaction[15] to give the NTz-based copolymer, PNTz4T. The polymer is soluble in warm chlorinated benzenes such as chlorobenzene (CB) and *o*-dichlorobenzene (DCB), and the molecular weight evaluated by GPC at 140 °C is M_n = 52.6 kDa and M_w = 127 kDa with PDI of 2.4 (Table 1).

Table 1. Chemical and Thermal Properties of the Polymers

polymer	M_n (kDa)[a]	M_w (kDa)[a]	PDI[a]	DP_n[b]	T_m (°C)[c] heating/cooling
PNTz4T	52.6	127	2.4	42.3	–
PBTz4T	36.1	114	3.2	35.2	185/170

[a]Determined by GPC using polystyrene standard and DCB as the eluent at 140 °C. [b]Based on the repeating unit. [c]Melting point determined by DSC measurements at a scan rate of 10 °C/min.

For comparison, we also synthesized a BTz-based polymer with 2-octyldodecyl side chains, PBTz4T. 3-(2-Octyldodecyl)-5-trimethylstannylthiophene (**2**) and 4,7-dibromo-2,1,3-benzothiadiazole (**6**) were cross-coupled to give BTz2T, and then the dibromination was followed to yield BTz-based comonomer **7**. **7** was then polymerized with **5** to provide PBTz4T. PBTz4T has the molecular weight of M_n = 36.1 kDa (M_w = 114 kDa, PDI = 3.2) and is soluble in chloroform. In addition, 3-methyl-5-trimethylstannylthiophene was cross-coupled with **3** and **6**, with the same procedure as NTz2T and BTz2T, to give NTz2T-Me and BTz2T-Me, respectively.

The thermal properties of the polymers were evaluated by differential scanning calorimetry (DSC). Figure 2 shows the

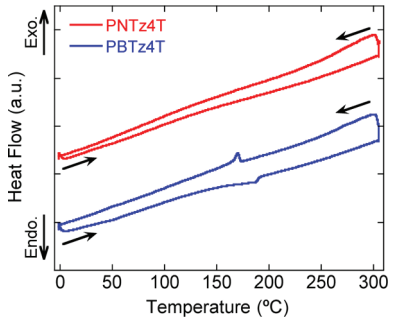

Figure 2. DSC thermograms of the polymers.

DSC thermograms of PNTz4T and PBTz4T. While PNTz4T did not show transition peaks below 300 °C, PBTz4T had a melting peak at 185 and 170 °C in the heating and cooling processes, respectively, which implies that PNTz4T is more rigid than PBTz4T.

Characterization of the Monomers and the Model Compounds. Optical and electrochemical characterizations were carried out with NTz2T and BTz2T, the actual monomer units for the polymers. UV−vis absorption spectra of NTz2T and BTz2T in the chloroform solution are shown in Figure 3a, and the optical data are summarized in Table 2. Indeed, NTz2T, with the NTz core, gave the absorption maximum (λ_{max}) at 491 nm, which is 28 nm longer than that for BTz2T, with the BTz core (463 nm). E_g values for these compounds determined from the absorption onset are 2.26 and 2.32 eV, respectively. Interestingly, the absorption coefficient is higher in NTz2T than in BTz2T, indicating that NTz affords not only broad but also strong absorption.

Cyclic voltammetry (CV) was carried out with NTz2T and BTz2T in the solution (Figure 3b), and their onset redox potentials (E_{red}^{onset} and E_{ox}^{onset}), LUMO energy levels (E_{LUMO}), and E_{HOMO} are summarized in Table 2. As expected, NTz2T gave a higher oxidation potential, thus deeper E_{HOMO} = −5.54 eV, than BTz2T (E_{HOMO} = −5.46 eV), and a higher reduction potential, thus higher E_{LUMO} = −3.52 eV, than BTz2T (E_{LUMO} = −3.42 eV), indicating stronger electron affinity of NTz as compared to BTz. These E_{HOMO} values are fairly consistent with the theoretical MO calculations of the corresponding model compounds, NTz2T-Me and BTz2T-Me, by the DFT method, where they provide −5.52 and −5.40 eV, respectively (Figure 4).

Single-crystal X-ray analysis was performed using the model compounds with the methyl substituent on thiophene, NTz2T-Me and BTz2T-Me, instead of NTz2T and BTz2T with the long branched alkyl substituents, since it is difficult to prepare single crystals of NTz2T and BTz2T. The analysis revealed that both molecules are mostly coplanar (Figure 5), where for NTz2T-Me the dihedral angle between the thiophene ring and the NTz core is 7.4°, and for BTz2T-Me that between thiophene and BTz is 5.6°. It is interesting to note that the configuration of the attached thiophenes and the NTz or BTz core is fixed, where the sulfur atoms in the thiophene rings point in the opposite direction to the thiadiazole rings, probably minimizing the steric impact between the hydrogen atoms on the thiophene rings and the NTz or BTz core. As a consequence, in NTz2T-Me, the thiophene rings that sandwich NTz are arranged in the *anti* manner, whereas, in BTz2T-Me, the thiophene rings are arranged in the *syn* manner. The difference of the arrangement, which originates in the different symmetry between NTz (centrosymmetry) and BTz (axisymmetry), seems to influence largely the ordering structure of the polymers, which will be discussed later.

Physicochemical Properties of the Polymers. UV−vis absorption spectra of the polymers in the solution and in the film are shown in Figure 6. In the polymer solution (Figure 6a), PNTz4T showed λ_{max} = 707 nm, with an absorption coefficient of 8.7 × 10^4, which significantly blue-shifted to 616 nm upon heating, indicating strong aggregation even in the solution. In the warm solution, which reflects the extent of π-conjugation of the single polymer chain, λ_{max} = PNTz4T (616 nm) was located at 66 nm longer wavelength region than that of PBTz4T, 552 nm, suggesting that the substitution of BTz for NTz extends π-conjugation. As consistent with the results in NTz2T and BTz2T, the absorption coefficients of PNTz4T were about twice as those of PBTz4T. The wider absorption range and the larger absorption coefficients, compared to those of PBTz4T, imply the better light-harvesting ability of PNTz4T, and hence should be beneficial for solar cell applications. In the thin film, PNTz4T exhibited λ_{max} = 725 nm, about 60 nm red-shifted from that of PBTz4T (Figure 6b). Furthermore, in PNTz4T, the longer wavelength region of the absorption peak at λ_{max} appears sharper as compared to PBTz4T, indicating better molecular ordering, likely due to its rigid π-extended structure. The absorption onset in the thin film for PNTz4T is

dx.doi.org/10.1021/ja210687r | J. Am. Chem. Soc. 2012, 134, 3498−3507

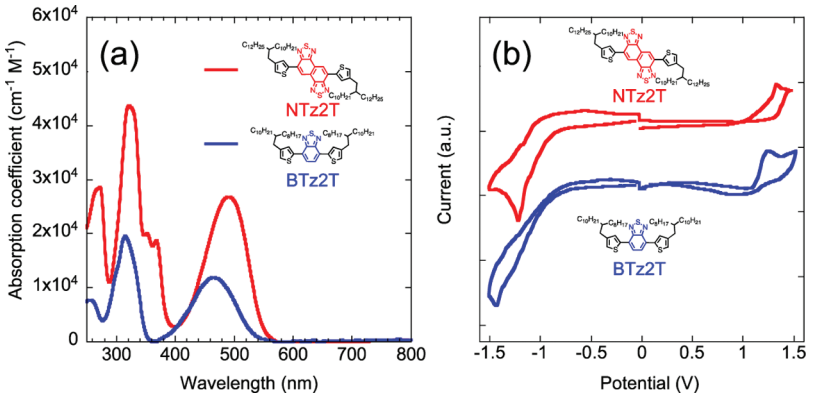

Figure 3. (a) UV−vis absorption spectra and (b) cyclic voltammograms of NTz2T and BTz2T in solution (chloroform for UV and dichloromethane for CV).

Table 2. Optical and Electrochemical Properties

compound	λ_{max} (nm) solution[a] rt/heat	λ_{max} (nm) film[b]	E_g (eV)[c] UV−vis/CV	E_{red}^{onset} (V)[d]	E_{LUMO} (eV)[e]	E_{ox}^{onset} (V)[d]	E_{HOMO} (eV)[e]	IP (eV)[f]
NTz2T	491/−	−	2.26/2.02	−1.28	−3.52	0.74	−5.54	−
BTz2T	463/−	−	2.32/2.04	−1.38	−3.42	0.66	−5.46	−
PNTz4T	707/616	725	1.54/1.39	−1.03	−3.77	0.36	−5.16	5.20
PBTz4T	572/550	662	1.65/1.54	−1.27	−3.53	0.27	−5.07	5.15

[a]Absorption maxima in the solution at room temperature/at around 80 °C. [b]Absorption maxima in the thin film. [c]Energy bandgaps determined from absorption onset/cyclic voltammetry. [d]Onset potentials (V vs Ag/AgCl) from reduction (E_{red}^{onset}) and oxidation (E_{ox}^{onset}). All the potentials were calibrated with the Fc/Fc$^+$ ($E^{1/2}$ = +0.43 V measured under identical conditions). [e]Estimated with the following equation: $E_{LUMO} = -4.80 - E_{red}^{onset}$; $E_{HOMO} = -4.80 - E_{ox}^{onset}$. [f]Determined by photoelectron spectroscopy in air.

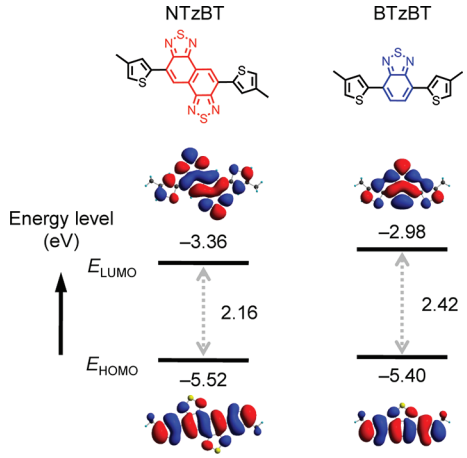

Figure 4. Calculated HOMOs and LUMOs of NTz2T-Me and BTz2T-Me.

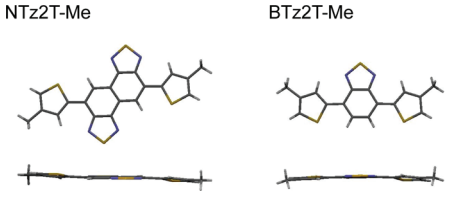

Figure 5. Molecular structures of NTz2T-Me and BTz2T-Me determined by single-crystal X-ray analysis.

determined to be 805 nm, with which E_g was calculated to be 1.54 eV, whereas that for PBTz4T was 1.65 eV.

E_{HOMO} of PNTz4T in the thin film was estimated to be −5.16 eV by CV, which is 0.09 eV deeper than that of PBTz4T (Figure 7a), as seen in the comonomer units. On the other hand, E_{LUMO} values for PNTz4T and PBTz4T were −3.77 and −3.53 eV, and the difference between them E_{LUMO} values (0.24 eV) was larger than that of E_{HOMO}, resulting in a smaller electrochemical HOMO−LUMO gap of 1.39 eV for PNTz4T than for PBTz4T (1.54 eV), which suggests that the replacement of BTz with NTz has a greater influence on the LUMO than the HOMO. Ionization potentials (IPs) were also evaluated by photoelectron spectroscopy in air (Figure 7b) using polymer thin films, and IP for PNTz4T is determined to be 5.20 eV, which is 0.05 eV larger than that of PBTz4T, in good agreement with the electrochemical results. In addition, E_{HOMO} of the polymers are in good agreement with those obtained from the MO calculation using the model compounds of the polymer repeat units (NTz4T and BTz4T), which show −5.15 and −5.04 eV, respectively (Figure S2). MO calculations also predicted that the HOMO coefficients are fully distributed over the molecule, as is the case in NTz2T-Me and BTz2T-Me, which is believed to be favorable for the efficient hole transport through π-orbital interactions (Figure S2).[2f,17]

OFET Application. Transistor characteristics of the polymers were evaluated using top-contact, bottom-gate devices fabricated by using polymer thin films spin-coated from DCB solutions onto hexamethyldisilazane (HMDS)-modified and 1*H*,1*H*,2*H*,2*H*-perfluorodecyltriethoxysilane (FDTS)[16,17]-modified Si/SiO_2 substrates, which were subsequently annealed at 200 °C. PNTz4T had a very good film forming property, as it consistently formed uniform films even on substrates with a very low surface energy, such as the FDTS-modified substrate. Figure 8 depicts typical transfer and output curves of the PNTz4T- and PBTz4T-based devices with the FDTS-modified substrate. In both polymer devices, the transfer curves give negligible hysteresis (Figure 8a), and the output

dx.doi.org/10.1021/ja210687r | J. Am. Chem. Soc. 2012, 134, 3498−3507

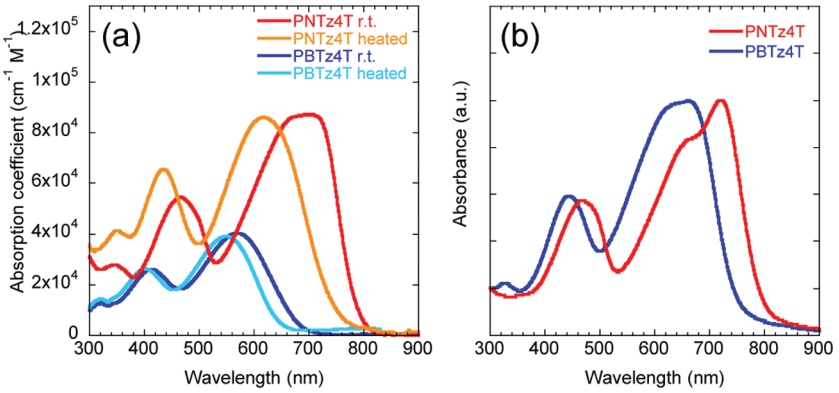

Figure 6. UV−vis absorption spectra of the polymers (a) in the solution (CB) and (b) in the thin film.

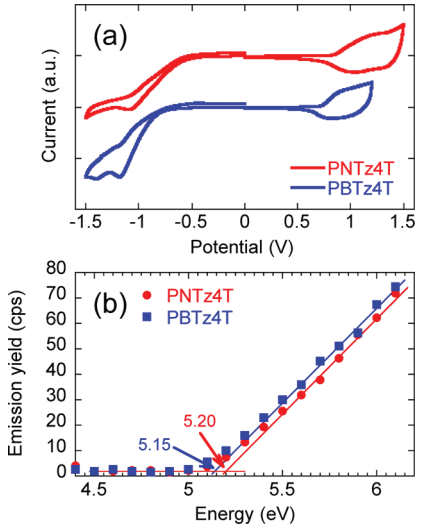

Figure 7. (a) Cyclic voltammograms and (b) photoelectron spectra of the polymer thin films.

curves show small contact resistance, as there are slight nonlinear behaviors in the low V_{DS} region (Figure 8b,c). Mobilities evaluated at the saturation regime for PNTz4T were as high as 0.56 cm^2/(V s) and typically in a range of 0.2−0.4 cm^2/(V s), with current on/off ratios of ~10^7 (Table 3). The mobility of PNTz4T was 1 order of magnitude higher than that of PBTz4T, typically 0.05 cm^2/(V s), indicating the high potential of the NTz core. OFETs with the HMDS-modified substrate showed trends similar to those with the FDTS-modified substrate, where the mobility for PNTz4T was ~0.35 cm^2/(V s) and for PBTz4T was ~0.021 cm^2/(V s). The slightly high mobility in OFETs with the FDTS-modified substrate is perhaps due to the better orientation of the polymers.[18]

Solar Cell Application. Solar cells were fabricated by spin-coating the polymer/$PC_{61}BM$ solutions, with appropriate polymer-to-$PC_{61}BM$ (p:n) ratios, in DCB onto the PEDOT:PSS spin-coated ITO glass, followed by vacuum evaporation of LiF/Al as the cathode. $J-V$ curves of the devices under 1 sun of simulated AM 1.5G solar irradiation (100 mW/cm^2) and the external quantum efficiency (EQE) spectra are displayed in Figure 9, and photovoltaic parameters are summarized in Table 4. While PBTz4T showed the best PCE of 2.6% at p:n = 1:1, with J_{SC} = 5.6 mA/cm^2, V_{OC} = 0.74 V, and FF = 0.63, PNTz4T showed the best PCE of 6.3% at p:n = 1:1.5, with J_{SC} = 12.0 mA/cm^2, V_{OC} = 0.76 V, and FF = 0.69. PNTz4T-based cells with p:n =1:1 and 1:2 also showed PCEs of >5.5%, which decreased to <4.5% with lower J_{SC} of about 8 mA/cm^2 at p:n = 1:3. Significantly higher J_{SC} for the devices with PNTz4T than with PBTz4T is most likely as a result of, in part, the wider absorption range and possibly the larger absorption coefficients of PNTz4T. In fact, devices with both polymers show photoresponse in the range of the absorption spectra, and the PNTz4T-device provides higher EQEs relative to the PBTz4T-devices, consistent with the J_{SC} values (Figure 9b). V_{OC} values of the PNTz4T-devices were similar to those of the PBTz4T-devices, which could be reasonable because the

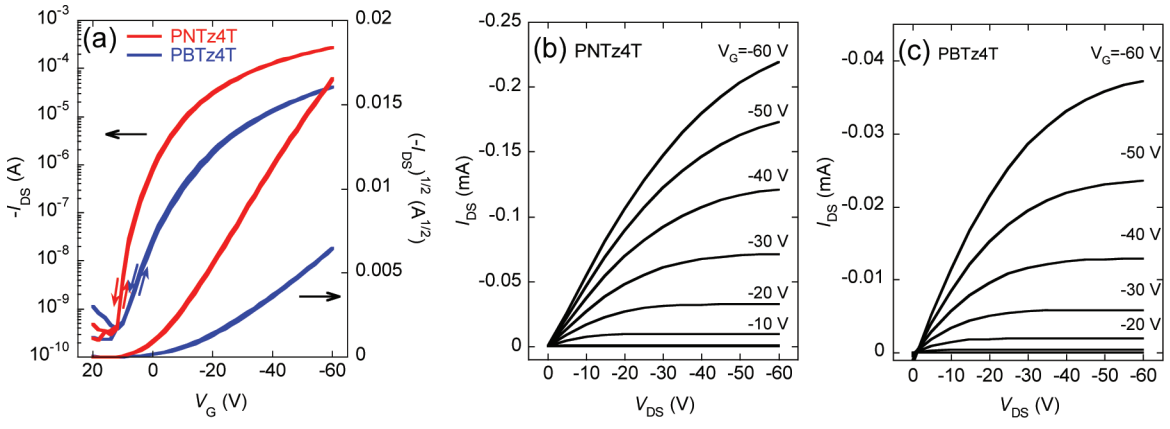

Figure 8. Typical transfer curves of OFETs (a), and output curves of PNTz4T-based (b) and PBTz4T-based (c) devices.

dx.doi.org/10.1021/ja210687r | J. Am. Chem. Soc. 2012, 134, 3498−3507

Table 3. Transistor Properties of the Polymers

	HMDS			FDTS		
polymer	μ (cm^2/(V s))[a]	V_T (V)	I_{on}/I_{off}	μ (cm^2/(V s))[a]	V_T (V)	I_{on}/I_{off}
PNTz4T	~0.35	−12 to −6	~10^7	~0.56	−10 to −2	~10^7
PBTz4T	~0.021	−12 to −8	~10^6	~0.074	−8 to −5	~10^5

[a]Maximum hole mobility calculated from the saturation regime (V_{DS} = −60 V).

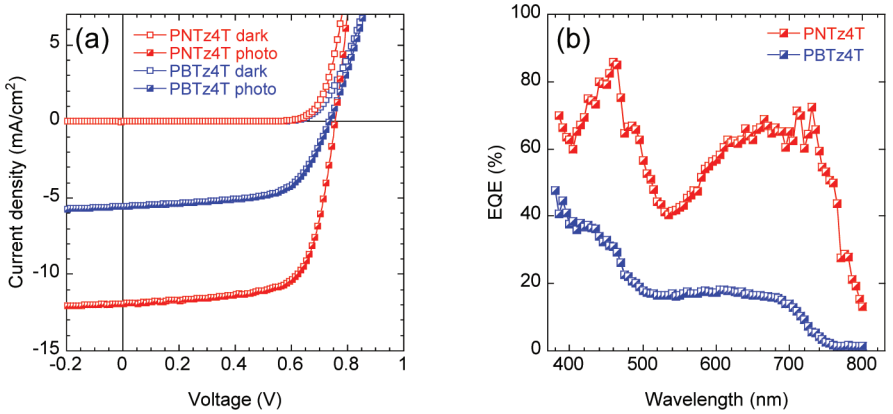

Figure 9. J–V curves (a) and EQE spectra (b) of BHJ solar cells (ITO/PEDOT:PSS/polymer:$PC_{61}BM$/LiF/Al); polymer:$PC_{61}BM$ = 1:1.5 for PNTz4T and 1:1 for PBTz4T.

Table 4. Photovoltaic Properties of the Polymer-Based Solar Cells

polymer	p:n[a]	J_{SC} (mA/cm^2)	V_{OC} (V)	FF	PCE (%)
PNTz4T	1:1	12.4	0.76	0.61	~5.6
	1:1.5	12.0	0.76	0.69	~6.3
	1:2	11.6	0.74	0.67	~5.9
	1:3	8.7	0.74	0.71	~4.4
PBTz4T	1:1	5.6	0.74	0.63	~2.6
	1:2	3.1	0.76	0.62	~1.5

[a]Polymer (p) to $PC_{61}BM$ (n) weight ratio.

difference in E_{HOMO} between the polymers is very small (0.05 eV).

Molecular Ordering in the Thin Films. In order to further understand these higher performances for PNTz4T and the striking difference in the device performances between PNTz4T and PBTz4T, the ordering structures in the thin film were investigated by X-ray diffraction studies. Two-dimensional grazing incidence X-ray diffraction (2D-GIXD) images of PNTz4T and PBTz4T films on the FDTS-modified SiO_2 substrate, which reflect the ordering structure in the transistors, are shown in Figure 10a,b. In PNTz4T, diffractions assignable to the lamellar ($q_z \approx 0.25$ Å^{-1}) and the π–π stacking structures ($q_{xy} \approx 1.7$ Å^{-1}) appear on the q_z and q_{xy} axes, respectively, indicating the predominant edge-on orientation on the substrate surface, though there are some misoriented fractions, most likely as a result of the introduction of long branched alkyl groups in the side chain.[9c] In contrast, PBTz4T showed largely arcing diffraction corresponding to the lamellar structure, indicating that there is no preferential orientation. PBTz4T did not show clear diffraction corresponding to the π–π stacking structure, indicative of the much lesser crystalline nature of PBTz4T in the thin film. Comparisons of the ordering structure between PNTz4T and PBTz4T were also performed using out-of-plane and in-plane X-ray diffraction (XRD). It is obvious from the patterns of polymer-only films (Figure 10c, red lines) that PNTz4T shows well-ordered structure, though, again, it contains misoriented (face-on) fractions, as the lamellar (2θ = 3.7°) and π–π stacking (2θ = 25.3°) peaks appear in the in-plane and out-of-plane patterns, respectively. The π–π stacking distance (d_π) of PNTz4T determined by the in-plane XRD pattern was 3.5 Å, which is very narrow for semiconducting polymers, and thus this well rationalizes the high mobilities of PNTz4T-based OFETs. Meanwhile, in PBTz4T (blue lines), although there are lamellar peaks, the π–π stacking signal is almost absent, suggesting that PBTz4T is much less crystalline. This large difference in the ordering structure between PNTz4T and PBTz4T is in good agreement with the fact that the OFET performances are quite distinct.

Polymer/$PC_{61}BM$ blend films on the PEDOT:PSS-coated ITO glass substrate were also subjected to the 2D-GIXD and XRD measurements to investigate the ordering structure in the solar cells. The p:n ratio of the films used in this study is same as their best cells. In the 2D-GIXD image of the PNTz4T/$PC_{61}BM$ (1:1.5) blend film, it is found that PNTz4T mainly orients in a face-on manner, as the diffraction corresponding to the π–π stacking appears on the q_z axis (Figure 10d). The enhanced face-on orientation of PNTz4T in the blend film is also evident from the XRD patterns (Figure 10f, red lines); the π–π stacking peak in the out-of-plane appears more strongly than in the in-plane, and thus the blend film contains mainly face-on crystallites and some edge-on crystallites and/or misoriented crystallites. Such a drastic change of the orientation by blending with $PC_{61}BM$ has also been seen in the TzTz-polymer system.[9e] It should also be noted that PNTz4T still has the narrow d_π = 3.5 Å in the blend film. In the meantime, PBTz4T provides much less crystalline feature in the blend film, where there is no π–π stacking diffraction in both the 2D-GIXD image (Figure 10e) and the XRD pattern (Figure 10f, blue lines). The predominant face-on orientation and the preserved narrow d_π of PNTz4T in the blend film should allow efficient orthogonal charge transport in the cells,[6d,19] which could be one of the main reasons that PNTz4T shows high

dx.doi.org/10.1021/ja210687r | J. Am. Chem. Soc. 2012, 134, 3498–3507

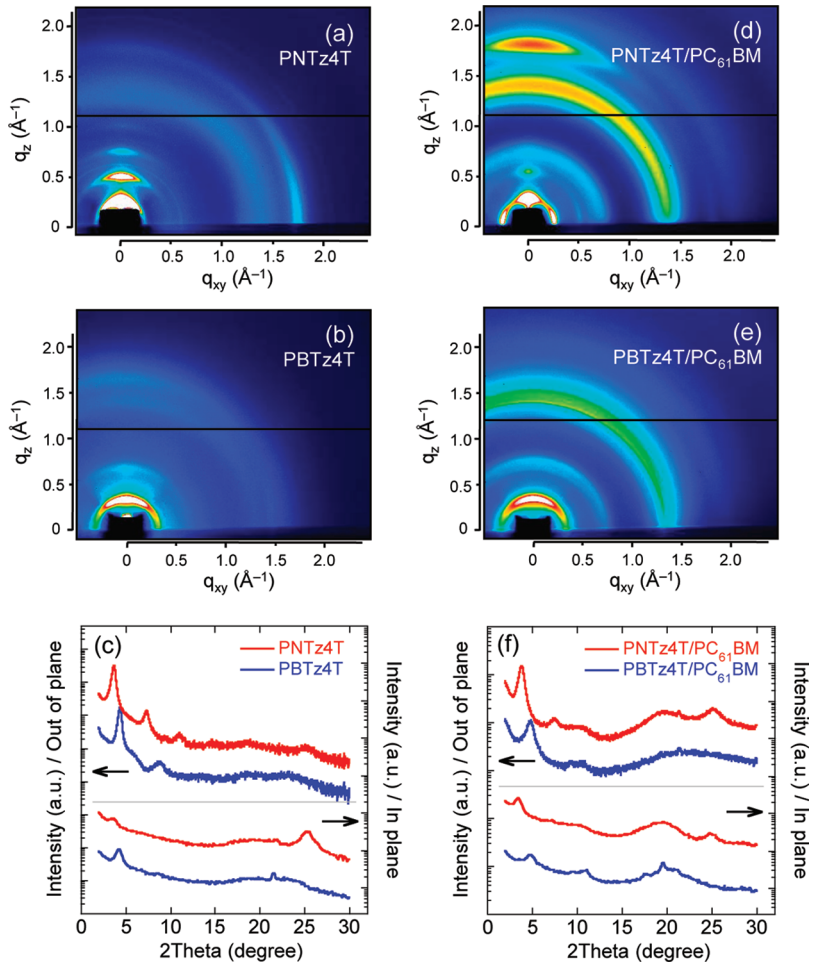

Figure 10. 2D-GIXD images of the PNTz4T thin film (a), PBTz4T thin film (b), PNTz4T/$PC_{61}BM$ blend film (d), and PBTz4T/$PC_{61}BM$ blend film (e). Out-of-plane and in-plane XRD patterns of the polymer-only films (red line, PNTz4T; blue line, PBTz4T) (c), and polymer/$PC_{61}BM$ blend films (red line, PNTz4T; blue line, PBTz4T) (f). The polymer-only films were cast on the FDTS-modified Si/SiO_2 substrate and subsequently annealed at 200 °C, and the polymer/$PC_{61}BM$ blend films were cast on the ITO glass/PEDOT:PSS substrate.

PCE of exceeding 6% and greater performances as compared to PBTz4T with a less ordered structure.

Why Is the $\pi-\pi$ Stacking Structure between PNTz4T and PBTz4T So Different? NTz is a more highly extended fused ring as compared to BTz, and thus it is fairly acceptable that PNTz4T forms a more highly ordered structure as compared to PBTz4T. However, the difference in crystallinity, especially the $\pi-\pi$ stacking, between the present two polymers in both the polymer-only film and the blend film is markedly large. We speculate that this marked difference originates in the difference of symmetry between the NTz and BTz unit.[20] As shown by the single-crystal X-ray analysis of NTz2T-Me and BTz2T-Me in an earlier section, the NTz (or BTz)−thiophene linkage is fixed in one configuration; NTz, with a centrosymmetrical structure, affords an *anti* arrangement of the thiophene rings that sandwich NTz, whereas BTz, with an axisymmetrical structure, affords a *syn* arrangement of the neighboring thiophenes (Figure 5). Based on these arrangements, PNTz4T gives a more linear-shaped backbone as compared to PBTz4T, which gives a "wavy" shape (Figure 11). The backbone shape might largely affect the packing structure, and we believe that this relatively linear backbone shape, together with the rigidity of NTz, leads to the highly ordered packing structure in the thin film in PNTz4T.[17,21] In addition, the alkyl

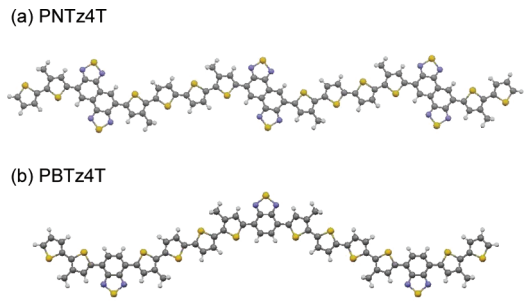

Figure 11. Optimized backbone structures of (a) PNTz4T and (b) PBTz4T.

side chains always alternate pointing up and down, and this could also contribute to the better molecular ordering.

It is interesting to note that a similar BTz-based copolymer with a quarter thiophene donor unit, but with different alkyl chain placement (POD2T-DTBT),[8b] is reported to show field-effect mobilities of ~0.20 $cm^2/(V\,s)$ and PCEs of ~5.9% (with $PC_{61}BM$, ~6.3% is reported when $PC_{71}BM$ is used). As has been shown in some polythiophene-based polymers, the side-chain placement significantly affects the crystalline structure,[22] and thus we speculate that POD2T-DTBT possibly forms a better ordering structure than PBTz4T due to the same reason,

dx.doi.org/10.1021/ja210687r | J. Am. Chem. Soc. 2012, 134, 3498−3507

though we do not fully understand the nature because XRD analysis for POD2T-DTBT was not reported in the literature. This, however, implies that BTz has some limitation on the choice of donor units when designing semiconducting polymers in order to achieve high performances. In contrast, NTz may not have such limitation and thus could be a more versatile unit for high-performance semiconducting polymers.

CONCLUSION

We have shown that a novel semiconducting polymer based on NTz (PNTz4T), a doubly BTz fused heteroaromatic, synthesized in this work exhibits not only high field-effect mobilities of exceeding 0.5 $cm^2/(V\,s)$ but also high photovoltaic properties with PCEs of ∼6.3%, demonstrating great promise for use of the polymer in organic electronic devices. These values are far better than those for the BTz counterpart (PBTz4T). With NTz's strong electron affinity, PNTz4T showed wide absorption ranging from 350 to 800 nm and a relatively low-lying E_{HOMO} of −5.2 eV, ca. 60 nm red-shifted from and ca. 0.1 eV deeper than the values for PBTz4T. A striking structural feature of PNTz4T is the strong $\pi-\pi$ stacking structure with a narrow distance of 3.5 Å. The crystallinity of PNTz4T is found to be markedly higher than PBTz4T in both the polymer-only film and the $PC_{61}BM$ blend film, which likely originates in the difference of symmetry of the cores. While NTz, with centrosymmetry, leads to a straighter backbone along with a favorable side-chain placement, BTz, with axisymmetry, provides a "wavy" backbone when combined with the quaterthiophene unit, which might significantly differ ordering structures in the thin film. Due to its strong electron affinity and its highly π-extended and centrosymmetric structure, NTz is a promising building block in the development of high-performance semiconducting polymers for both transistors and solar cells.

EXPERIMENTAL SECTION

Materials. 3-(2-Decyltetradecyl)-5-trimethylstannylthiophene (**1**) and 3-(2-octyldodecyl)-5-trimethylstannylthiophene (**2**),[23] 4,9-dibromonaphtho[1,2-*c*:5,6-*c*′]bis[1,2,5]thiadiazole (**3**),[14] 5,5′-bis-(trimethylstannyl)-2,2′-bithiophene,[24] 4,7-bis(5-bromo-4-(2-octyldodecyl)thiophen-2-yl)benzo[*c*][1,2,5]thiadiazole (**7**)[23] were synthesized according to the reported procedure, respectively. All chemicals and solvents were of reagent grade unless otherwise indicated. THF was purified by a glass contour solvent system (Nikko Hanssen & Co., Ltd.), and toluene was distilled with CaH_2 prior to use. Polymerization was carried out with a microwave reactor (Biotage Initiator). NMR spectra were obtained in deuterated chloroform and 1,2-dichlorobenzene (DCB, for polymers) with TMS as internal reference. EI-MS spectra were obtained on a Shimadzu QP-2010SE spectrometer using an electron impact ionization procedure (70 eV). Molecular weights were determined by gel permeation chromatography (GPC) with a TOSOH HLC-8121GPC/HT instrument at 140 °C using DCB as a solvent and calibrated with polystyrene standards.

4,9-Bis(4-(2-decyltetradecyl)thiophen-2-yl)naphtho[1,2-c:5,6-c′]bis[1,2,5]thiadiazole (NTz2T). **1** (584 mg, 1.0 mmol) and **3** (201 mg, 0.5 mmol) were added to 25 mL of toluene in a 100 mL three-neck flask and purged with N_2 for 30 min. Tetrakis(triphenylphosphine)-palladium(0) (11.5 mg, 0.01 mmol) was added to the mixture, which was then refluxed for 15 h. After the mixture cooled to room temperature, aqueous KF was added, and the aqueous layer was extracted with dichloromethane. The organic layer was washed with water and brine and then dried over anhydrous $MgSO_4$. After removal of the solvent by vacuum evaporation, the residue was purified by column chromatography on silica gel with hexane−dichloromethane (2:1), followed by recrystallization from ethyl acetate to give NTz2T as a red solid (454 mg, 84% yield). ^{1}H NMR (400 MHz, $CDCl_3$): δ 8.99 (s, 2H), 8.10 (d, 2H, J = 1.2 Hz), 7.10 (d, 2H, J = 1.2 Hz), 2.67 (d, 4H, J = 6.8 Hz), 1.74 (m, 2H), 1.15−1.40 (m, 80H), 0.80−0.90 (m, 12H). ^{13}C NMR (100 MHz, $CDCl_3$): δ 153.5, 152.5, 143.2, 138.4, 130.4, 126.7, 124.7, 123.4, 122.0, 38.9, 35.1, 33.3, 31.9, 30.1, 29.7, 29.7, 29.7, 29.4, 29.4, 26.7, 22.7, 14.1. MALDI-TOF-MS: m/z = 1081.77 (M^+). Anal. Calcd for $C_{66}H_{104}N_4S_4$: C, 73.28; H, 9.6; N, 5.18. Found: C, 73.47; H, 9.83; N, 5.14.

*4,9-Bis(5-bromo-4-(2-decyltetradecyl)thiophen-2-yl)naphtho[1,2-c:5,6-c′]bis[1,2,5]thiadiazole (**4**).* *N*-Bromosuccinimide (89 mg, 0.5 mmol) was added portionwise to a solution of NTz2T (270 mg, 0.25 mmol) in 15 mL of THF at 0 °C. After the mixture was stirred for 4 h at room temperature, $NaHCO_3$ solution was added, and the mixture was extracted with dichloromethane. The organic layer was washed with water and brine and then dried over anhydrous $MgSO_4$. The solvent was removed by vacuum evaporation, and the residue was purified by column chromatography on silica gel with hexane−dichloromethane (2:1), followed by recrystallization from ethyl acetate to give **4** as a red solid (242 mg, 78% yield). ^{1}H NMR (400 MHz, $CDCl_3$): δ 8.76 (s, 2H), 7.85 (s, 2H), 2.59 (d, 4H, J = 7.1 Hz), 1.79 (m, 2H), 1.15−1.40 (m, 80H), 0.80−0.90 (m, 12H). ^{13}C NMR (100 MHz, $CDCl_3$): δ 153.1, 152.0, 142.4, 137.9, 129.4, 125.7, 124.5, 121.3, 113.3, 38.6, 34.3, 33.4, 31.9, 30.1, 29.7, 29.7, 29.7, 29.4, 26.6, 22.7, 14.1. MALDI-TOF-MS: m/z = 1239.43 (M^+). Anal. Calcd for $C_{66}H_{104}N_4S_4Br_2$: C, 63.95; H, 8.29; N, 4.52. Found: C, 63.79; H, 8.13; N, 4.54.

PNTz4T. **4** (124 mg, 0.1 mmol), **5** (49.2 mg, 0.1 mmol), tetrakis(triphenylphosphine)palladium(0) (2.3 mg, 2 μmol), and toluene (5 mL) were added to a 20 mL reaction vial. The vial was purged with argon and subsequently sealed. The vial was heated in a microwave reactor at 180 °C for 40 min. After cooling to room temperature, the reaction mixture was poured into a mixture of methanol (100 mL) and concentrated hydrochloric acid (5 mL) and vigorously stirred for 6 h at room temperature. The precipitate was filtered and subjected to Soxhlet extraction with methanol, hexane, chloroform, and finally chlorobenzene. The chlorobenzene fraction was concentrated and poured into methanol. The precipitate was isolated by filtration and dried *in vacuo* to afford the polymer sample (117 mg, 94%) as a metallic black solid. Anal. Calcd for $C_{74}H_{108}N_4S_6$: C, 71.44; H, 8.59; N, 4.50. Found: C, 71.06; H, 8.55; N, 4.43. GPC (DCB, 140 °C): M_n = 52 600, M_w = 127 000, PDI = 2.41.

PBTz4T. **7** (102 mg, 0.1 mmol), **5** (49.2 mg, 0.1 mmol), tetrakis(triphenylphosphine)palladium(0) (2.3 mg, 2 μmol), and toluene (5 mL) were added to a 20 mL reaction vial. The vial was purged with argon and subsequently sealed. The vial was heated in a microwave reactor at 180 °C for 40 min. After cooling to room temperature, the reaction mixture was poured into a mixture of methanol (100 mL) and concentrated hydrochloric acid (5 mL) and vigorously stirred for 6 h at room temperature. The precipitate was filtered and subjected to Soxhlet extraction with methanol, hexane, and finally chloroform. The chloroform fraction was concentrated and poured into methanol. The precipitate was isolated by filtration and dried *in vacuo* to afford the polymer sample (87 mg, 85%) as a metallic black solid. Anal. Calcd for $C_{62}H_{92}N_2S_5$: C, 72.74; H, 8.86; N, 2.74. Found: C, 72.05; H, 8.82; N, 2.69. GPC (DCB, 140 °C): M_n = 36 100, M_w = 11 400, PDI = 3.16.

Instrumentation and Calculation. UV−vis absorption spectra were measured using a Shimadzu UV-3600 spectrometer. Thermal analyses were carried out with differential scanning calorimetry (DSC) on a Shimadzu DSC-60 instrument at 10 °C/min for both heating and cooling processes. Ionization potential (IP) was determined from the onset of photoelectron spectra measured by using a photoelectron spectrometer, model AC-2, in air (Riken Keiki Co., Ltd). Dynamic force-mode atomic force microscopy study was carried out on a Nanocute scanning probe microsope system (SII Nanotechnology, Inc.). GIXD experiments were conducted at the SPring-8 on beamline BL19B2. The sample was irradiated at a fixed incident angle on the order of 0.12° through a Huber diffractometer, and the GIXD patterns were recorded with a 2-D image detector (Pilatus 100K). GIXD patterns were recorded with an X-ray energy of 12.39 keV (λ = 1 Å). Two images were taken in each measurement due to the limited range

dx.doi.org/10.1021/ja210687r | J. Am. Chem. Soc. 2012, 134, 3498−3507

of the detector, and thus two images are layered to show the entire pattern; a lateral black line in each GIXD image is to show the changeover. Out-of-plane and in-plane X-ray diffraction specular scans were carried out using a Rigaku Ultima IV instrument. Samples for the X-ray measurements were prepared by drop-casting the polymer solution on the FDTS-modified Si/SiO_2 substrate and the polymer/$PC_{61}BM$ solution on the PEDOT:PSS spin-coated ITO glass.

OFET Fabrication and Measurement. OFET devices were fabricated in a "top-contact" configuration on heavily doped n^+-Si (100) wafers with 200-nm-thick thermally grown SiO_2 (C_i = 17.3 nF/cm^2). The Si/SiO_2 substrates were carefully cleaned and then treated with HMDS or FDTS to form a self-assembled monolayer, in which the silicon wafers were exposed to FDTS vapor in a closed desiccator. Polymer layers were then spin-coated from warm (~80 °C) 3 g/L DCB solution at 1000 rpm for 10 s and then 2500 rpm for 45 s and subsequently annealed at 150 °C for 30 min under nitrogen. On top of the polymer thin films, Au drain and source electrodes (thickness 80 nm) were deposited in a vacuum through a shadow mask, where the drain−source channel length (L) and width (W) are 50 μm and ca. 1.5 mm, respectively. Current−voltage characteristics of the OFET devices were measured at room temperature in air with a Keithly 4200-SCS semiconductor characterization system. Field-effect mobilities were calculated in the saturation regime (V_{DS} = −60 V) of the I_{DS} using the following equation,

$$I_{DS} = (WC_i/2L)\mu(V_G - V_T)^2$$

where C_i is the capacitance of the SiO_2 dielectric, I_{DS} is the source−drain current, and V_{DS}, V_G, and V_T are the source−drain, gate, and threshold voltages, respectively. Current on/off ratios (I_{on}/I_{off}) were determined from the minimum current around V_G = 0−20 V (I_{off}) and the current at V_G = −80 V (I_{on}). The mobility data were collected from more than 10 different devices.

Solar Cell Fabrication and Measurement. ITO substrates were first precleaned sequentially by sonicating in a detergent bath, deionized water, acetone, and isopropanol at room temperature and in a boiled isopropanol bath, each for 10 min. They were then subjected to a UV/ozone treatment at room temperature for 20 min. The precleaned ITO substrates were coated with PEDOT:PSS (Clevios P VP Al4083) by spin-coating (7000 rpm for 30 s, thickness ~50 nm), and then baked at 130 °C for 10 min under N_2 atmosphere. The photoactive layer was deposited in air by spin-coating a DCB solution containing 5 mg/mL of the polymer sample with a respective amount of $PC_{61}BM$ passed through a 0.45 μm poly(tetrafluoroethylene) filter at 400 rpm for 20 s and 1500 rpm for 5 s, followed by drying in a vacuum for 2 h. The counter electrode, consisting of LiF (0.8 nm) and Al (100 nm), was deposited by vacuum evaporation, where the active area of the cells was 0.0314 cm^2. The thickness of the film was measured using a surface profiler (Ambios XP-100). $J-V$ characteristics were measured using a Keithley 2400 source-measure unit in air without encapsulation of the cells under 1 sun (AM1.5G) conditions using a solar simulator (Asahi Spectra, HAL-320, JIS class AAA) at 100 mW/cm^2. EQE spectra were measured with a home-built setup consisting of an Asahi Spectra HAL-320 Xe lamp in combination with an Asahi Spectra CMS-100 monochromator. The number of photons incident on the device was calculated for each wavelength by using a calibrated Si diode as the reference.

■ ASSOCIATED CONTENT

Supporting Information

Complete ref 2f, device characteristics, and surface morphologies of the polymers. This material is available free of charge via the Internet at http://pubs.acs.org.

■ AUTHOR INFORMATION

Corresponding Author

iosaka@hiroshima-u.ac.jp; ktakimi@hiroshima-u.ac.jp

Notes

The authors declare no competing financial interest.

■ ACKNOWLEDGMENTS

This work is supported by the Strategic Promotion of Innovative Research and Development from the Japan Science and Technology Agency (JST), the New Energy and Industrial Technology Development Organization (NEDO), and Grants-in-Aid for Young Scientist B (No. 22750172) and Grants-in-Aid for Scientific Research A (No. 23245041) from Japan Society for the Promotion of Science (JSPS). I.O. is also grateful to the Sumitomo Foundation and the JGC-S Scholarship Foundation for financial support. GIXD experiments were performed at the BL19B2 of SPring-8 with the approval of the Japan Synchrotron Radiation Research Institute (JASRI) (Proposal No. 2011A1735 and 2011B1860).

■ REFERENCES

(1) (a) Skotheim, T. A.; Reynolds, J. R. *Handbook of Conducting Polymers*, 3rd ed.; CRC Press: Boca Raton, FL, 2007. (b) Leclerc, M.; Morin, J.-F. *Design and Synthesis of Conjugated Polymers*; Wiley-VCH Verlag GmbH & Co. KGaA: Weinheim, Germany, 2010. (c) Arias, A. C.; MacKenzie, J. D.; McCulloch, I.; Rivnay, J.; Salleo, A. *Chem. Rev.* **2010**, *110*, 3−24. (d) Facchetti, A. *Chem. Mater.* **2011**, *23*, 733−758. (e) Garnier, F.; Hajlaoui, R.; Yassar, A.; Srivastava, P. *Science* **1994**, *265*, 1864−1866. (f) Brabec, C.; Dyakonov, V.; Scherf, U. *Organic Photovoltaics, Materials Device Physics, and Manufacturing Technologies*; Wiley-VCH Verlag GmbH & Co. KGaA: Weinheim, Germany, 2008. (g) Günes, S.; Neugebauer, H.; Sariciftci, N. S. *Chem. Rev.* **2007**, *107*, 1324−1338. (h) Thompson, B. C.; Frechet, J. M. J. *Angew. Chem., Int. Ed.* **2008**, *47*, 58−77. (i) Peet, J.; Heeger, A. J.; Bazan, G. C. *Acc. Chem. Res.* **2009**, *42*, 1700−1708. (j) Chen, J.; Cao, Y. *Acc. Chem. Res.* **2009**, *42*, 1709−1718. (k) Inganäs, O.; Zhang, F.; Andersson, M. R. *Acc. Chem. Res.* **2009**, *42*, 1731−1739. (l) Liang, Y.; Yu, L. *Acc. Chem. Res.* **2010**, *43*, 1227−1236. (m) Boudreault, P.-L. T.; Najari, A.; Leclerc, M. *Chem. Mater.* **2011**, *23*, 456−469. (n) Facchetti, A. *Chem. Mater.* **2011**, *23*, 733−758.

(2) (a) Hamadani, B. H.; Gundlach, D. J.; McCulloch, I.; Heeney, M. *Appl. Phys. Lett.* **2007**, *91*, 243512. (b) Umeda, T.; Kumaki, D.; Tokito, S. *J. Appl. Phys.* **2009**, *105*, 024516. (c) Tsao, H. N.; Cho, D.; Andreasen, J. W.; Rouhanipour, A.; Breiby, D. W.; Pisula, W.; Müllen, K. *Adv. Mater.* **2009**, *21*, 209−212. (d) Zhang, W.; Smith, J.; Watkins, S. E.; Gysel, R.; McGehee, M.; Salleo, A.; Kirkpatrick, J.; Ashraf, S.; Anthopoulos, T.; Heeney, M. *J. Am. Chem. Soc.* **2010**, *132*, 11437−11439. (e) Li, Y.; Singh, S. P.; Sonar, P. *Adv. Mater.* **2010**, *22*, 4862−4866. (f) Bronstein, H.; et al. *J. Am. Chem. Soc.* **2011**, *133*, 3272−3275. (g) Tsao, H. N.; Cho, D. M.; Park, I.; Hansen, M. R.; Mavrinskiy, A.; Yoon, D. Y.; Graf, R.; Pisula, W.; Spiess, H. W.; Müllen, K. *J. Am. Chem. Soc.* **2011**, *133*, 2605−2612.

(3) (a) Liang, Y.; Xu, Z.; Xia, J.; Tsai, S.; Wu, Y.; Li, G.; Ray, C.; Yu, L. *Adv. Mater.* **2010**, *22*, E135−E138. (b) Chen, H. Y.; Hou, J.; Zhang, S.; Liang, Y.; Yang, G.; Yang, Y.; Yu, L.; Wu, Y.; Li, G. *Nature Photon.* **2009**, *3*, 649−653. (c) Chu, T. Y.; Lu, J.; Beaupré, S.; Zhang, Y.; Pouliot, J. R.; Wakim, S.; Zhou, J.; Leclerc, M.; Li, Z.; Ding, J.; Tao, Y. *J. Am. Chem. Soc.* **2011**, *133*, 4250−4253. (d) Price, S. C.; Stuart, A. C.; Yang, L.; Zhou, H.; You, W. *J. Am. Chem. Soc.* **2011**, *133*, 4625−4631.

(4) Sirringhaus, H.; Brown, P. J.; Friend, R. H.; Nielsen, M. M.; Bechgaard, K.; Langeveld-Voss, B. M. W.; Spiering, A. J. H.; Janssen, R. A. J.; Meijer, E. W.; Herwig, P.; De Leeuw, D. M. *Nature* **1999**, *401*, 685−688.

(5) (a) Mühlbacher, D.; Scharber, M.; Morana, M.; Zhu, Z.; Waller, D.; Gaudiana, R.; Brabec, C. *Adv. Mater.* **2006**, *18*, 2884−2889. (b) Zhang, M.; Tsao, H. N.; Pisula, W.; Yang, C.; Mishra, A. K.; Müllen, K. *J. Am. Chem. Soc.* **2007**, *129*, 3472−3473.

(6) (a) Pan, H.; Li, Y.; Wu, Y.; Liu, P.; Ong, B. S.; Zhu, S.; Xu, G. *J. Am. Chem. Soc.* **2007**, *129*, 4112−4113. (b) Liang, Y.; Wu, Y.; Feng, D.; Tsai, S. T.; Son, H. J.; Li, G.; Yu, L. *J. Am. Chem. Soc.* **2009**, *131*,

56−57. (c) Zou, Y.; Najari, A.; Berrouard, P.; Beaupré, S.; Badrou, R. A.; Tao, Y.; Leclerc, M. *J. Am. Chem. Soc.* **2010**, *132*, 5330−5331. (d) Piliego, C.; Holcombe, T. W.; Douglas, J. D.; Woo, C. H.; Beaujuge, P. M.; Fréchet, J. M. J. *J. Am. Chem. Soc.* **2010**, *132*, 7595−7597. (e) Zhang, Y.; Hau, S. K.; Yip, H.-L.; Sun, Y.; Acton, O.; Jen, A. K.-Y. *Chem. Mater.* **2010**, *22*, 2696−2698.

(7) Chen, Y.-C.; Yu, C.-Y.; Fan, Y.-L.; Hung, L.-I.; Chen, C.-P.; Ting, C. *Chem. Commun.* **2010**, *46*, 6503−6505.

(8) (a) Hou, J.; Chen, H. Y.; Zhang, S.; Li, G.; Yang, Y. *J. Am. Chem. Soc.* **2008**, *130*, 16144−16145. (b) Ong, K. H.; Lim, S. L.; Tan, H. S.; Wong, H. K.; Li, J.; Ma, Z.; Moh, L. C. H.; Lim, S. H.; de Mello, J. C.; Chen, Z. K. *Adv. Mater.* **2011**, *23*, 1409−1413.

(9) (a) Osaka, I.; Sauvé, G.; Zhang, R.; Kowalewski, T.; McCullough, R. D. *Adv. Mater.* **2007**, *19*, 4160−4165. (b) Osaka, I.; Zhang, R.; Sauvé, G.; Smilgies, D.-M.; Kowalewski, T.; McCullough, R. D. *J. Am. Chem. Soc.* **2009**, *131*, 2521−2529. (c) Osaka, I.; Zhang, R.; Liu, J.; Smilgies, D.-M.; Kowalewski, T.; McCullough, R. D. *Chem. Mater.* **2010**, *22*, 4191−4196. (d) Huo, L.; Guo, X.; Zhang, S.; Li, Y.; Hou, J. *Macromolecules* **2011**, *44*, 4035−4037. (e) Osaka, I.; Saito, M.; Mori, H.; Koganezawa, T.; Takimiya, K. *Adv. Mater.* **2012**, *24*, 425−430.

(10) Guo, X.; Ortiz, R. P.; Zheng, Y.; Kim, M.-G.; Zhang, S.; Hu, Y.; Lu, G.; Facchetti, A.; Marks, T. J. *J. Am. Chem. Soc.* **2011**, *133*, 13685−13697.

(11) (a) Bürgi, L.; Turbiez, M.; Pfeiffer, R.; Bienewald, F.; Kirner, H.; Winnewisser, C. *Adv. Mater.* **2008**, *20*, 2217−2224. (b) Wienk, M. M.; Turbiez, M.; Gilot, J.; Janssen, R. A. J. *Adv. Mater.* **2008**, *20*, 2556−2560.

(12) (a) Stalder, R.; Mei, J.; Reynolds, J. R. *Macromolecules* **2010**, *43*, 8348−8352. (b) Lei, T.; Cao, Y.; Fan, Y.; Liu, C.-J.; Yuan, S.-C.; Pei, J. *J. Am. Chem. Soc.* **2011**, *133*, 6099−6101. (c) Wang, E.; Ma, Z.; Zhang, Z.; Vandewal, K.; Henriksson, P.; Inganäs, O.; Zhang, F.; Andersson, M. R. *J. Am. Chem. Soc.* **2011**, *133*, 14244−14247.

(13) Mataka, S.; Takahashi, K.; Ikezaki, Y.; Hatta, T.; Tori-i, A.; Tashiro, M. *Bull. Chem. Soc. Jpn.* **1991**, *64*, 68−73.

(14) Wang, M.; Hu, X.; Liu, P.; Li, W.; Gong, X.; Huang, F.; Cao, Y. *J. Am. Chem. Soc.* **2011**, *133*, 9638−9641.

(15) Tierney, S.; Heeney, M.; McCulloch, I. *Synth. Met.* **2005**, *148*, 195−198.

(16) Osaka, I.; Abe, T.; Shinamura, S.; Takimiya, K. *J. Am. Chem. Soc.* **2011**, *133*, 6852−6860.

(17) (a) Kobayashi, S.; Nishikawa, T.; Takenobu, T.; Mori, S.; Shimoda, T.; Mitani, T.; Shimotani, H.; Yoshimoto, N.; Ogawa, S.; Iwasa, Y. *Nat. Mater.* **2004**, *3*, 317−322. (b) Nakayama, K.; Uno, M.; Nishikawa, T.; Nakazawa, Y.; Takeya, J. *Org. Electron.* **2010**, *11*, 1620−1623. (c) Osaka, I.; Takimiya, K.; McCullough, R. D. *Adv. Mater.* **2010**, *22*, 4993−4997.

(18) Umeda, T.; Kumaki, D.; Tokito, S. *J. Appl. Phys.* **2009**, *105*, 024516.

(19) (a) He, F.; Wang, W.; Chen, W.; Xu, T.; Darling, S. B.; Strzalka, J.; Liu, Y.; Yu, L. *J. Am. Chem. Soc.* **2011**, *133*, 3284−3287. (b) Rivnay, J.; Steyrleuthner, R.; Jimison, L. H.; Casadei, A.; Chen, Z.; Toney, M. F.; Facchetti, A.; Neher, D.; Salleo, A. *Macromolecules* **2011**, *44*, 5246−5255.

(20) Rieger, R.; Beckmann, D.; Mavrinskiy, A.; Kastler, M.; Müllen, K. *Chem. Mater.* **2010**, *22*, 5314−5318.

(21) He, M.; Li, J.; Tandia, A.; Sorensen, M.; Zhang, F.; Fong, H. H.; Pozdin, V. A.; Smilgies, D.-M.; Malliaras, G. G. *Chem. Mater.* **2010**, *22*, 2770−2779.

(22) (a) Ong, B. S.; Wu, Y.; Li, Y.; Liu, P.; Pan, H. *Chem.—Eur. J.* **2008**, *14*, 4766−4778. (b) He, M.; Li, J.; Sorensen, M.; Zhang, F.; Hancock, R.; Fong, H. H.; Pozdin, V. A.; Smilgies, D.-M.; Malliaras, G. G. *J. Am. Chem. Soc.* **2009**, *131*, 11930−11938.

(23) Lu, J.; Liang, F.; Drolet, N.; Ding, J.; Tao, Y.; Movileanu, R. *Chem. Commun.* **2008**, 5315−5317.

(24) Seitz, D. E.; Lee, S. H.; Hanson, R. N.; Bottaro, J. C. *Synth. Commun.* **1983**, *13*, 121.